Environmental context sculpts spatial and temporal visual processing in thalamus

Kayla Peelman[1], Bilal Haider[1*]

[1]Dept of Biomedical Engineering, Georgia Institute of Technology & Emory University, Atlanta, GA, USA

*Lead contact: bilal.haider@bme.gatech.edu

Abstract

Behavioral state modulates neural activity throughout the visual system; this is largely due to changes in arousal that alter internal brain state. However, behaviors are constrained by the external environmental context, so it remains unclear if this context itself dictates the regime of visual processing, apart from ongoing changes in arousal. Here, we addressed this question in awake head-fixed mice while they passively viewed visual stimuli in two different environmental contexts: either a cylindrical tube, or a circular running wheel. We targeted high-density silicon probe recordings to the dorsal lateral geniculate nucleus (dLGN) and simultaneously measured several electrophysiological and behavioral correlates of arousal changes, and thus controlled for them across contexts. We found surprising differences in spatial and temporal processing in dLGN across contexts, even in identical states of alertness and stillness. The wheel context (versus tube) showed elevated baseline activity, faster visual responses, and smaller but less selective spatial receptive fields. Further, arousal caused similar changes to visual responsiveness across all conditions, but the environmental context mainly changed the overall set-point for this relationship. Together, our results reveal an unexpected influence of the physical environmental context on fundamental aspects of visual processing in the early visual system.

Introduction

Sensory responses in the brain depend on the behavioral context in which they occur. For example, visual responses to the exact same stimuli differ if they occur in periods of low versus high alertness[1-3]. Moreover, even during behavioral tasks with identical visual stimuli, neural responses in the same brain area differ according to the physical environmental context of the task[4]. These studies suggest that the overall effects of behavioral context on neural responses could reflect both internal context (e.g., alertness, body movement, etc.), but also external environmental context (e.g., properties of physical surfaces, their spatial layout, visual characteristics, etc.). The influence of internal context on neural visual processing has been investigated in great detail in the mouse visual system[5-8], but there is comparatively much less known about the influence of external environmental context, and how this shapes neural visual processing[9].

A first question about environmental context and visual processing concerns how the choice of experimental set-up effectuates body movement. The mouse visual system evolved to support active, locomoting visual behaviors such as navigation[10,11], hunting[12], and evasion[13-15], and many studies have revealed the effects of locomotion on visual processing in awake head-fixed mice placed on a floating ball[2,5,8], or circular treadmill[16,17]. In such studies, neural responses throughout the visual system differ greatly during periods of locomotion versus stillness[2,5,18], as does the quality of behavioral task performance[3,7]. For these reasons, many studies instead place head-fixed mice on rigid platforms or inside cylindrical tubes to mitigate the influences of locomotion (and consequences of movement) on neural activity[19-26]. However, it remains unknown if the choice of experimental set-up creates an environmental context that itself shapes the regime of visual processing, and if potential differences across contexts are mainly due to the promotion or prevention of locomotion. A first step towards clarifying this would be to measure neural responses to the same visual stimuli — in different environmental contexts — but focusing on periods of stillness, to better isolate effects of environmental context on visual processing.

Second, could any effects of environmental context be explained simply by changes to internal brain state? It is well-known that changes in brain state can lead to significant differences in both baseline and evoked firing in visual areas[5,7,8,27]. Likewise, it is well-known that locomotion induces widespread changes to brain state, mediated largely through the recruitment of neuromodulatory systems[18,28-31]. Thus, it may be the case that even in periods of stillness, certain environmental contexts (e.g., a wheel that permits locomotion) promote fundamentally different brain states than others (e.g., a tube that prevents locomotion). To clarify

this, it would be beneficial to measure visual responses during periods of stillness in two different environmental contexts, while tracking moment-to-moment changes in brain state; this could determine if effects of environmental context on visual processing arise largely through changes in brain state.

Third, if environmental context itself influences visual processing, where in the visual system might this happen? Sensitivity to behavioral context is usually attributed to cortical areas[32,33], but recent evidence in mice suggests that contextual modulation occurs throughout the visual system[8,34,35]. In the mouse dorsal lateral geniculate nucleus (dLGN), locomotion increases baseline and visually evoked activity[8,36], and alertness strongly influences temporal processing[17]; further, inactivation of dLGN diminishes signals associated with movement and arousal in primary visual cortex (V1), suggesting that thalamocortical activity may play a key role in contextual modulation[37]. This work suggests that dLGN may also be sensitive to environmental context, and in a key position to broadcast the effects throughout the feedforward visual hierarchy[38-40].

Here, we addressed these questions about visual processing and environmental context by measuring dLGN spiking in awake mice head-fixed in two different set-ups: either a partially enclosed cylindrical tube, or on a circular running wheel. In both cases, we only examined trials in which the animal was stationary. To disentangle the effects of environmental context from brain state changes, we used classical measures of cortical local field potential power to identify epochs with similar levels of alertness across the two contexts. In these carefully controlled conditions, we found that even during periods of identical alertness and stillness, dLGN responses showed sensitivity to the environmental context in which they occurred. Compared to the tube context, the wheel context elevated ongoing baseline activity, improved visual response timing, and restricted spatial receptive field size in dLGN. Thus, even as early as the thalamus, environmental context itself appears to shape the regime of visual processing.

Results

Our goal was to determine whether the quality of visual processing in the dLGN depends upon external environmental context, independent from effects driven by differences in arousal. One hypothesis is that, regardless of the context, dLGN visual processing is largely explained by arousal state; an alternative is that context itself engenders different qualities of visual processing even during identical states of arousal (Fig. 1A,B).

To test these hypotheses, we placed awake, head-fixed mice in two distinct environmental contexts: a semi-enclosed plastic cylinder ("Tube" group; N = 7 mice), or on a circular treadmill in which mice were free to locomote or remain stationary ("Wheel" group; N = 5 mice). Experiments were often performed in both contexts in the same mice (5/9 mice were recorded from in both contexts). On the wheel, we verified well-known effects of locomotion-induced arousal changes on dLGN visual processing (Figs. S1-S2), indicating the wheel context captures a behavioral repertoire investigated in many prior studies[8,36]. Here, we do not further investigate the effects of locomotion on visual processing. Instead, we focus on the most frequent behavioral epochs when mice were stationary on the wheel (72% of time; Fig. S2E), and compared these with mice stationary in the tube. This permits comparison of visual processing in two distinct contexts, and on trials with similar arousal levels (explained below), free from influences of ongoing locomotion itself (Fig. 1A-B).

We simultaneously recorded spiking in dLGN and local field potential (LFP) activity from higher visual areas of cortex using Neuropixels 1.0, along with high-speed video of the face and eye (Fig. 1C). To assess contextual effects on spatial and temporal receptive field (RF) responses of single neurons, we presented small, brief black and white squares (7°; 0.1s duration) in randomized locations throughout the contralateral visual hemifield. We identified trials with the preferred stimuli for each dLGN neuron (stimulus color and location eliciting maximal response; Methods), and responses to these stimuli are the main topic of this report.

Arousal levels during stationary trials were highly overlapping in the two contexts. We categorized arousal levels using the visual cortical LFP delta power (1-4 Hz), a "gold standard" electrophysiological signature of arousal that is tightly synchronized with thalamic activity[41,42], and changes in pupil size[43], thus providing a high temporal resolution measure of trial-by-trial arousal levels across the visual thalamocortical pathway. In both contexts, visual cortical delta power was significantly anti-correlated with pupil size, a well-known external indicator of arousal (Fig. 1D; delta power inverted for display). Importantly, although pupil size varied with arousal level, the effects we detail in the following sections could not be explained simply by more light entering the pupil (Fig. S3; controls in full darkness and with

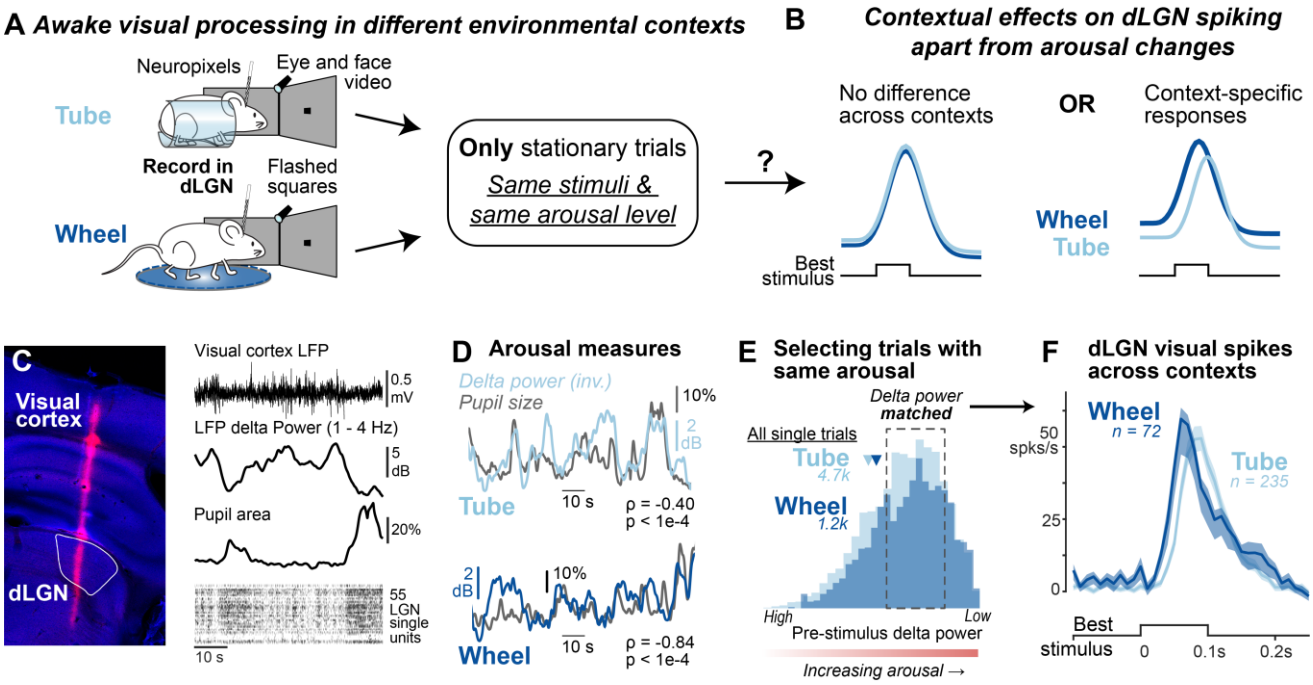

Figure 1. Measuring awake dLGN responses and arousal level in two different environmental contexts.

A. Awake, head-fixed mice were placed either in a tube (N=7 mice) or on circular treadmill (N=5 mice) while viewing full-contrast black or white squares (7°) presented one at a time for 0.1s in random locations across the visual hemifield. Neuropixels 1.0 probes simultaneously sampled neural activity across visual cortex and the dorsal lateral geniculate nucleus (dLGN). We examined only stationary trials on the wheel (72% of total, see Fig. S2) to isolate effects of context.
B. Schematic of two hypotheses for contextual effects. *Left,* visual responses in dLGN show no differences across context when arousal is the same. *Right,* dLGN responses show context-specificity even when arousal is the same.
C. *Left,* histological confirmation of probe track passing through visual cortex and targeting dLGN. *Right,* local field potential (LFP) and delta (1- 4 Hz) power was measured in visual cortex while single units were isolated in dLGN. Simultaneous high-speed video captured pupil and periocular motion.
D. Example traces of delta power (inverted) and pupil size across contexts. (Pearson correlation in tube ρ = -0.40, $p < 0.001$; wheel ρ = -0.84, $p < 0.001$).
E. Distribution of delta power preceding all analyzed visual stimulus trials in tube (light blue; 4734 trials) and wheel (dark blue; 1178 trials). Note that delta power axis is reversed (arranged high to low), so that arousal level increases from left to right.
F. dLGN neuron spike responses to the preferred stimulus in the receptive field across contexts (tube, n = 235 neurons; wheel n = 72 neurons).

pharmacologically dilated pupil). Trial-by-trial cortical delta power was highly overlapping across both contexts (Fig. 1E). We focused on the central 55% of trials surrounding the modal arousal level to determine the impact of context itself – apart from arousal level – on visual responses in dLGN.

To our surprise, in these carefully matched conditions, the overall dLGN spiking response to stimulation of the RF showed context specificity, with visibly faster and slightly stronger visual responses in stationary epochs on the wheel versus tube (Fig. 1F; wheel peak response is ~10 ms faster and evokes 4.8 more spikes per second relative to the tube). In the following sections, we quantify in detail how context governs the amplitude, timing, and selectivity of these responses.

Context adjusts visual response timing and baseline activity in dLGN

We first found that context influenced both baseline activity and visual response timing (Fig. 2A). Baseline activity was significantly greater on the wheel relative to the tube (Fig. 2B; all detailed quantifications in Figure legends throughout Results). After accounting for this large baseline difference, the peak visual response was not significantly different across contexts (Fig. 2C). However, visual response onset and peak response latencies were both significantly faster by ~10 ms on the wheel (Fig. 2D,E). The response duration was also significantly prolonged on the wheel (Fig. 2F). Overall, across all stationary epochs with highly overlapping arousal levels, visual responses were faster and more prolonged on the wheel than the tube.

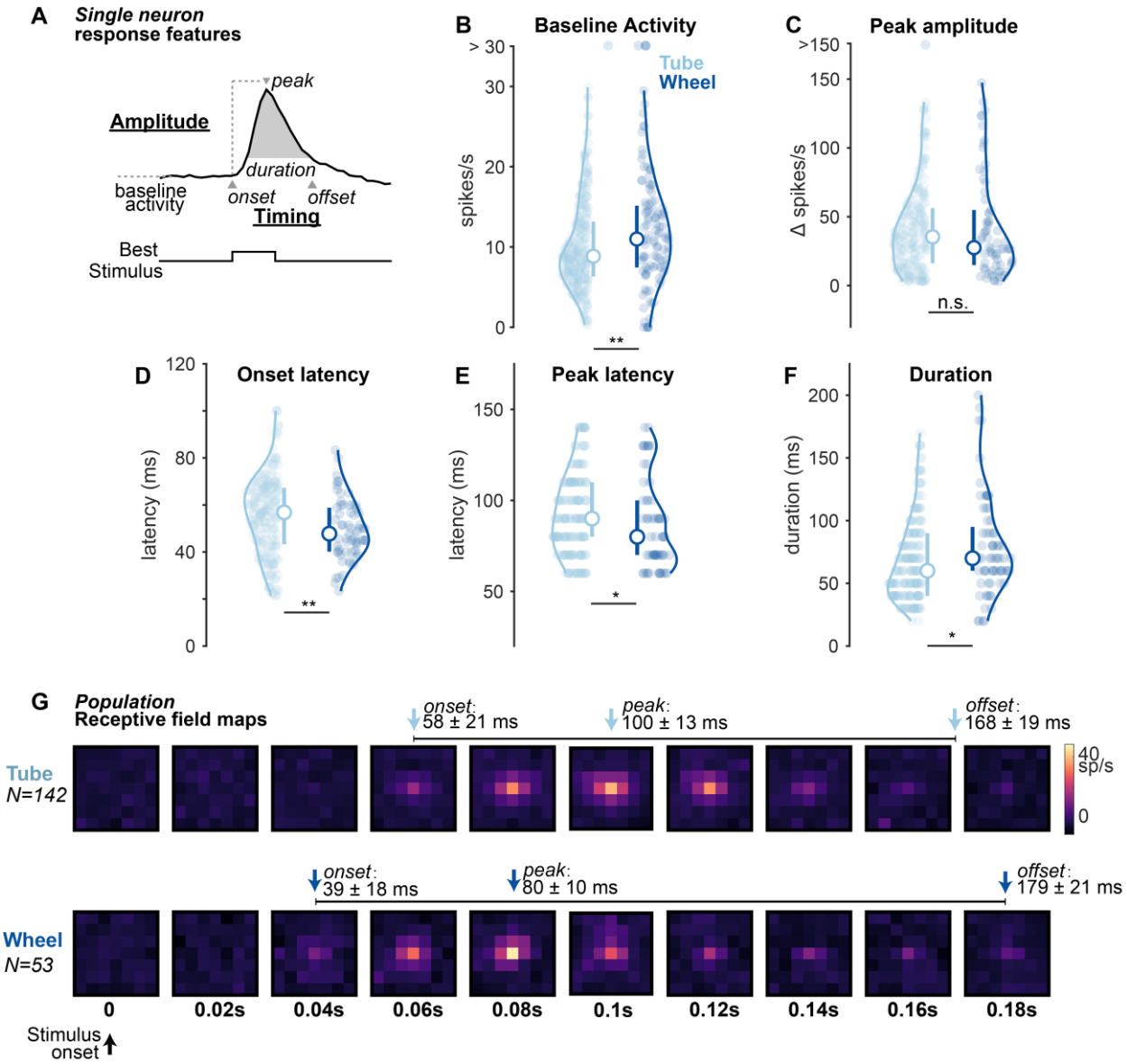

Figure 2. Environmental context influences visual response timing in dLGN

A. Schematic for quantification of visual response features (amplitude and timing) in dLGN across contexts.
B. Baseline activity was significantly elevated in the wheel context (wheel: 11.4 ± 4.1 spikes/s, n = 107; tube: 8.9 ± 3.4 spikes/s, n=276; p = 0.0018; Wilcoxon one-sided rank-sum test, Median ± IQR/2; same statistics throughout figure). Baseline calculated in 0.1s window prior to stimulus onset.
C. Baseline-subtracted peak visual response similar across contexts (wheel: Δ23.3 ± 18.9 spikes/s, n=72; tube: Δ30.7 ± 21.3 spikes/s, n=235; p = 0.088).
D. Onset latency significantly faster on the wheel (wheel: 47 ± 19 ms, tube: 57 ± 24 ms; p = 0.003).
E. Time to peak response significantly faster on the wheel (wheel: 87 ± 15 ms, tube: 93 ± 15 ms; p = 0.020)
F. Response duration significantly longer on wheel (wheel: 70 ± 25 ms, tube: 60 ± 20 ms; p = 0.025).
G. Population receptive field maps across time aligned to the center of each neuron's receptive field (top, tube n = 142 units; bottom, wheel n = 53). Population response onset and peak significantly faster on wheel (onsets: wheel, 39 ± 18; tube, 58 ± 21 ms; p = 0.002; peaks: wheel, 80 ± 10 ms; tube, 100 ± 13 ms; p = 0.044; Mean ± SD, permutation test; Methods). Response offset and overall duration (where activity was above 25% of the maximum response amplitude) not significantly different (tube 168 ± 19 ms, wheel 179 ± 2 ms, p = 0.360).

To better understand contextual effects on the timing of visual information transmitted by the LGN, and to ensure our findings were not due to individual sessions or mice, we generated population receptive field maps from neural ensembles recorded in each context (Fig. 2G; Methods). Surrogate populations were subsampled randomly from the entire recorded database to match the number of recordings in each context (17 in tube, 6 on wheel). Similar to the single neuron responses, we found that the population response onset and peak latencies were faster on the wheel, but duration was comparable. These

findings on response timing persisted when we equalized samples across contexts (data not shown here), and when we separately examined ON and OFF cells (ON cells: wheel, $p = 0.0475$; OFF cells: $p = 0.0184$). Taken together, context influences the level of ongoing activity and the speed of visual responses in dLGN at both the single neuron and population levels, even when arousal levels remain comparable.

Increasing arousal elevates baseline activity and improves response timing

The results so far demonstrate effects of context on visual processing when arousal levels were in an overlapping range. Does context also shape the way that changes in arousal level (i.e., increasing from low to high) affect dLGN visual responses? We addressed this by splitting the distribution of trials examined thus far into five equally sized bins, and arranged them from low to high arousal (Fig. 3A; Methods). To ensure that the definition of these bins remained independent of context, we combined all data across all recordings in both contexts and defined the bins according to the overall distribution of pre-stimulus cortical delta power. These bin definitions were then applied to each individual context for all comparisons (Fig. 3B, C).

We found that the influence of arousal level on dLGN activity exhibited similar directionality (i.e., increasing arousal drove increasing firing), but with significantly different set points across contexts. First, as expected, we found that increasing arousal level significantly elevated baseline activity for both contexts (Fig. 3D). This relationship was highly correlated on both the wheel and the tube, such that baseline activity was significantly greater at highest versus lowest arousal bins (Fig. 3E, F). However, regardless of arousal level, baseline activity was overall significantly greater on the wheel versus tube (Fig. 3D). Second, we found that increasing arousal level did not have a significant effect on visual response amplitude (Fig. 3G), with no clear difference on visual responses between highest and lowest arousal groups within context (Fig. 3H, I). Lastly, we found that increasing arousal significantly accelerated visual response onset latencies within context, (Fig. 3J), and these were again overall fastest on the wheel. Peak response latencies showed a similar form of arousal-induced modulation across contexts, and again overall these were fastest on the wheel (Fig. 3K). Response duration was significantly prolonged on the wheel, but invariant to increasing arousal levels within context (Fig. 3L). These findings on the relationship between increasing arousal and context were highly similar when we instead used other well-known measures of arousal to classify the trials (such as pupil size, narrowband gamma (NBG) power (50-70 Hz), and facial motion energy; Fig. S4). Taken together, our results show significant arousal-induced changes to baseline activity and visual response timing in dLGN even in stationary epochs, but with context-specific expression of these relationships.

Both context and arousal impact receptive field size & selectivity

Thus far, we have examined contextual effects on visual response amplitude and timing. Does context affect visual spatial resolution? First, we looked at how receptive field (RF) size and RF selectivity (Fig. 4A) differed across contexts (Fig. 4B,C; example units) at matched levels of arousal (same as in Figs. 1 and 2). We found that, overall, RF size was significantly smaller on the wheel (Fig. 4D). Overall RF selectivity (center versus background firing) was not different across the two contexts (Fig. 4E). We then examined how increasing arousal influenced these RF properties. In both contexts, as arousal increased so did RF size (Fig. 4F), and this significantly reduced RF selectivity (Fig. 4G). Furthermore, when examining how changes in arousal level effect RF size and selectivity, there emerged a significant effect of context: RFs were smaller but significantly less selective (relative to background activity) on the wheel. Thus, in both contexts, increasing arousal uniformly broadened RFs and lowered spatial selectivity. However, there remained a more specific effect of context on arousal-induced changes to RF properties: they were significantly smaller but less selective on the wheel versus the tube.

Discussion

Here we provide evidence that environmental context itself shapes visual processing in the dorsal lateral geniculate nucleus (dLGN). These effects were revealed by examining visual neural activity in identical states of alertness and only during periods of stillness. We found elevated background activity, faster visual responses, and smaller spatial receptive fields in a context that enabled locomotion (wheel), versus one that did not (tube). Taken together, our findings reveal an unexpected influence of the physical environment on fundamental aspects of neural processing in the dLGN, with implications for how such effects of the environment may be rapidly broadcast throughout the visual system.

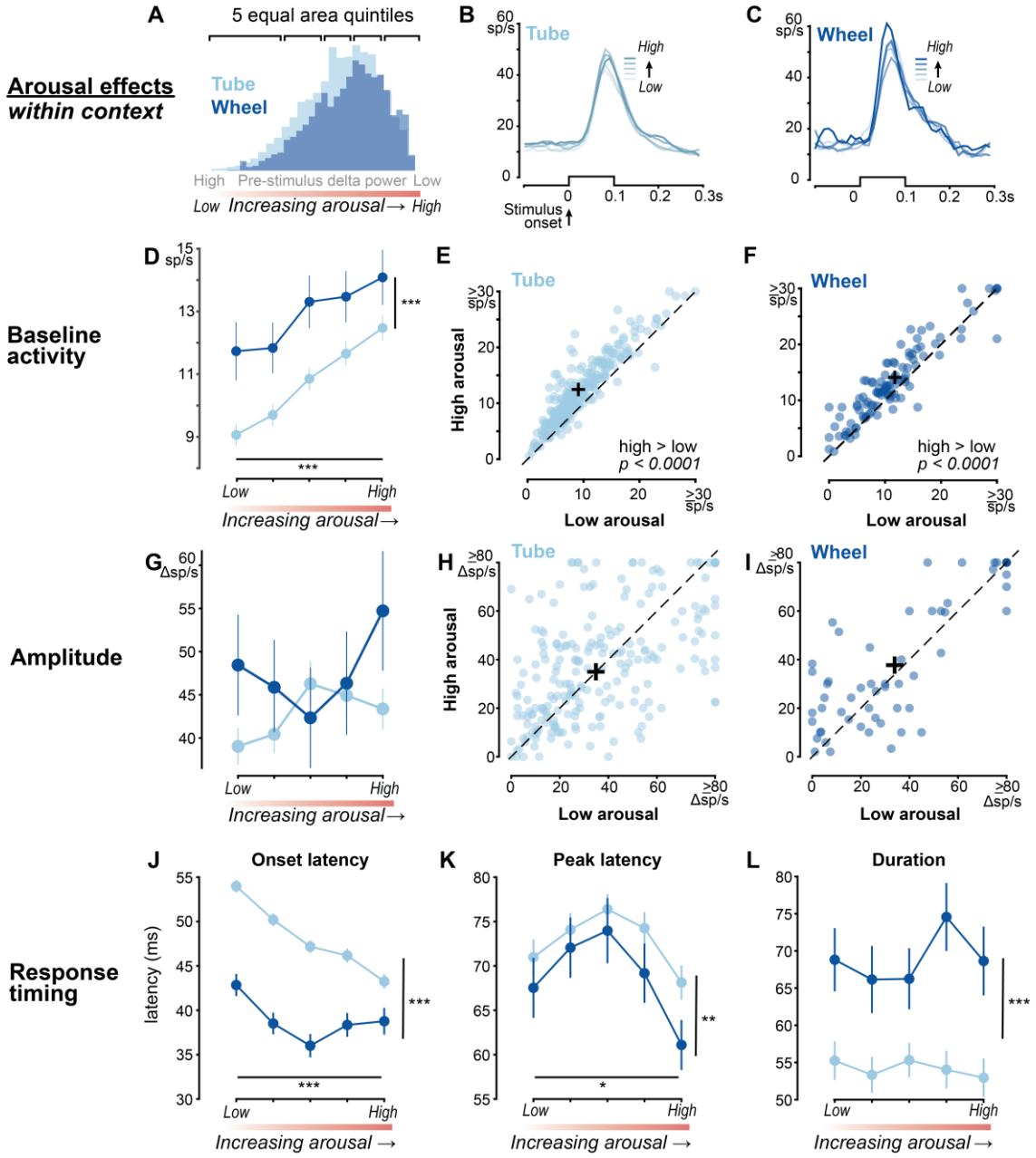

Figure 3. Impact of context on arousal-mediated changes of visual responses in dLGN

A. Pre-stimulus delta power distributions for tube (light) and wheel (dark) contexts divided into five equally sized bins to examine responses across increasing arousal level.
B. Average responses to best stimulus in the RF for tube (n=223 neurons), sorted by increasing arousal levels (line opacity) .
C. Same as in C, but on the wheel (n=63 neurons).
D. Significant effect of context (p = 2.2e-9) and arousal (p = 1.9e-6) on baseline activity (two-way ANOVA throughout figure unless indicated). Baseline activity increases with increasing arousal in both contexts (Spearman correlation, tube r = 1.00, p = 0.0167; wheel r = 1.0, p = 0.0167).
E. Baseline activity significantly greater at high versus low arousal in tube (low: 9.1 ± 0.3 spikes/s; high: 12.5 ± 0.4; p = 4.5e-41, Mean ± SEM; sign rank test).
F. Same as E, for wheel (low: 11.7 ± 0.9 spikes/s, high: 14.1 ± 0.9; p = 3.7e-8, sign rank test).
G. Baseline-subtracted visual response amplitude not significantly different with arousal level (p = 0.59) or context (p = 0.057).
H. Baseline-subtracted visual response amplitude similar for low versus high arousal levels in the tube (low: Δ39.0 ± 2.4 spikes/s, high: Δ 43.5 ± 2.6; p = 0.260, sign rank test).
I. Same as H, for wheel (low: Δ48.4 ± 6.0 spikes/s, high: Δ54.7 ± 7.0 spikes/s; p = 0.083, sign rank test).
J. Faster onset latency with increasing arousal (p = 2.92e-5) and is overall fastest on the wheel (p = 3.2e-19).
K. Time to peak response is overall faster in the wheel context (p = 0.02).
L. Response duration) is longer in the wheel context (p = 4.0e-9).

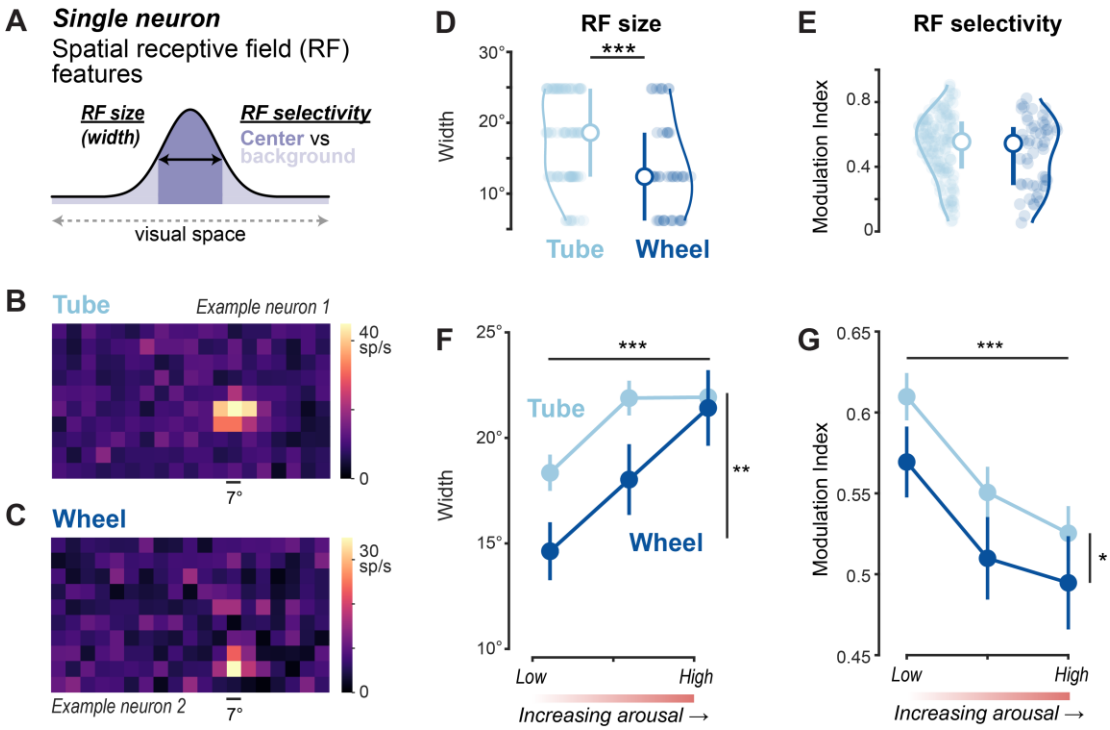

Figure 4. Context-specific effects on dLGN spatial RFs

A. Schematic showing estimation of spatial receptive field (RF) size. Width quantified as the extent of contiguous pixels on RF map that evoke ≥ 50% of the maximum amplitude. RF selectivity is quantified with a modulation index (MI) between the center and background [MI = (center - background) / (center + background)]. Center defined as the width at 50% maximum firing rate. No eye movements in any trials analyzed in this figure (Methods).
B. Example neuron RF map in the tube.
C. Example neuron RF map on the wheel.
D. At matched levels of arousal (as in Fig. 1E-F, Fig. 2), RF size is significantly smaller in the wheel (wheel 12 ± 7°, n=43; tube: 19 ± 7°, n = 90; p = 7.9e-3; Median ± IQR/2, Wilcoxon one-sided rank-sum test).
E. At matched levels of arousal, RF selectivity is similar between the tube and wheel contexts (tube: 0.6 ± 0.2; wheel: 0.5 ± 0.2, p = 0.260; Median ± IQR/2, Wilcoxon one-sided rank-sum test).
F. RF sizes significantly smaller on the wheel (p = 0.007). On both the tube and wheel, RF size significantly broadens with increasing arousal level (p = 0.0001; Mean ± SEM, two-way ANOVA).
G. RF selectivity is overall higher in the tube (p = 0.033) and selectivity worsens with increasing arousal across contexts (p = 0.0006; Mean ± SEM, two-way ANOVA).

An important feature of our experimental design was the focus on periods of stillness across contexts, when neural responses were free from the consequences of ongoing body-wide movement. The main difference between the two contexts was that one of them (wheel) permitted locomotion. However, stationary periods were the most frequent spontaneous behavioral state on the wheel (Fig. S2), facilitating comparison across the contexts. This natural propensity for stationary conditions is a common but often overlooked aspect of studies where mice are in a set-up that permits locomotion. In many studies, only periods of active locomotion are analyzed in order to ensure an active, engaged, low variability brain state[44-46]. In our experiments, reassuringly, we found the same locomotion-induced modulation of visual responses in dLGN on the wheel (Fig. S1, S2). However, since ongoing locomotion dramatically increases arousal level, and this affects both baseline and visually evoked firing in dLGN[8,36], this potentially obscures the more subtle effects of the environmental context on visual processing. Similarly, eye movements are the greatest during running[7,8], and could obscure interpretation of changes in spatial receptive field properties. These effects would be minimal during stationary trials, and we further eliminated any potential confounds of eye movements (Methods). Further, we were careful to restrict our analysis to those moments where the offset (or forthcoming onset) of running was >1 second away in time, since the cessation of running is followed by low-frequency thalamocortical oscillations that diminish visual responsiveness[30,37]. Thus, after carefully trying to account for these many well-known factors associated with locomotion, we were able to find that baseline visual processing was impacted by context, and that this was not simply predictable by large

differences in the momentary read out of brain state, using several different electrophysiological signatures.

Regardless of our choice of arousal measure – either neural or external – we observed an overall elevation in baseline firing and faster responses in the wheel context. We primarily categorized brain state with the simultaneously recorded visual cortical delta power (1-4 Hz) and categorized trials based on the brain state in the pre-stimulus period. Cortical delta power is a major correlate of arousal mediated changes to brain state[41] and low-frequency power co-fluctuates with changes in other arousal-related measures such as pupil size and locomotion onsets/offsets[2,43]. Critically, we examined several other ways to measure arousal, such as narrowband gamma (NBG) power in LGN[2,40,47], pupil size[43], and facial motion energy[37,48] (Fig. S3). All manners of arousal categorization revealed similar effects on baseline activity and response timing. Although we used transient stimuli and focused on response onsets, it has recently been shown that changes in arousal-related processes during wakefulness influence dLGN encoding of visual information at various timescales[49]. It is also important to note that we primarily categorized trials based on LFP from higher visual cortex, but again the main effects were consistent using other measures, including direct readouts of arousal (NBG power) in dLGN[38-40]. Our central finding of substantial changes in response timing (tens of milliseconds) at single neuron (Fig. 2A-F) and population levels (Fig. 2G) in different environmental contexts is broadly consistent with other studies showing millisecond-scale modulation of dLGN response timing[50]. Further, the two environmental contexts did not prevent how ongoing increases (or decreases) of arousal modulated response timing, baseline activity, or receptive field size; context mainly changed the overall set point for the relationships.

We found that in a context that permits locomotion, the visual system appears primed to process spatially localized information more quickly - even during total stillness. Further, we revealed that RF size increases as a function of increasing arousal even during stillness (Fig. 4F), echoing the effects previously observed with locomotion-induced arousal increases[8]. On the wheel, RF size was significantly smaller than on the tube; this coupled with faster latencies may allow for rapid and precise detection of high spatial frequency stimuli in an environment that enables locomotion— even during stationary epochs. Broad effects of environmental (and other) forms of context are known to affect the early visual system, and even impact feature processing at the level of the retina (e.g., spatial frequency tuning[34,36]). Our findings could imply that selectivity for visual attributes that themselves affect response latencies (e.g., spatial frequency[51]) could also differ across contexts, perhaps with further consequences for visuospatial selectivity and timing.

Several classical measures of brain state did not obviously explain the effects of the different contexts – so what factors might? Elevated baseline activity and faster responses on the wheel suggest that perhaps an overall DC depolarization of dLGN neurons drives the effects. Effects of DC depolarization may not be readily apparent in frequency-resolved electrophysiological measures within dLGN, nor in the cortical LFP readouts of brain state; likewise, they may not be apparent in slower external behavioral indicators of arousal such as pupil or facial motion. What could potentially drive this depolarization? A first possibility is cholinergic input, either directly or indirectly, through activation of the basal forebrain (BF). Indeed, tonic cholinergic stimulation slowly depolarizes dLGN neurons[52], and activation of BF increases baseline activity in dLGN and improves trial-by-trial visual response timing, enhancing reliability[53]; it is conceivable that cholinergic activity contributes to the different contextual effects on baseline activity and response timing in our experiments. An experiment to test this would be to record from dLGN in mice in the tube, then apply cholinergic agonists in dLGN locally (or by activation of the BF) and see if this mimics increased baseline activity and faster response latencies as found on the wheel. However, in monkey V1, acetylcholine shrinks RF size[54], unlike arousal mediated changes in mouse dLGN and in V1[8,55], possibly due to non-monotonic effects on excitability[43]. A second source of depolarization could be long-lasting activation of the mesencephalic locomotor region (MLR) that persists during stationary epochs on the wheel; for example, subtle activation of the parabrachial region within the MLR (that does not elicit locomotion) nonetheless reduces dLGN burst firing (a correlate of low arousal)[18,56]. A third potential source of depolarization is the noradenergic system; in V1, this maintains tonic depolarization during locomotion[30]; likewise, noradrenergic agonists in dLGN reduce burst firing[57-59]. Lastly, depolarization of dLGN neurons could arise from V1 feedback[17,60]. However, V1 provides both direct excitation and indirect inhibition of dLGN via the thalamic reticular nucleus, so this may not result in a straightforward, DC depolarization of dLGN[22,61]. Beyond the observed effects here of higher baseline activity and faster response timing, a context-mediated

depolarization could alter other aspects of visual processing. First, as argued above, depolarization could alter the degree of burst firing in different contexts[5,8,49]. Second, baseline depolarization could expand the dynamic range available to encode luminance changes[62,63]. For example, in OFF neurons, tonic depolarization would enable faster and stronger spiking to dark stimuli; in addition, the elevated baseline firing (due to depolarization) would heighten the firing rate "ceiling" (and increase the driving force for inhibition), so that suppression evoked by non-preferred bright stimuli would appear more intense, relative to the higher baseline. This regime may be advantageous for dLGN neurons to signal rapid changes in luminance in contexts that enable interleaved locomotion and stillness. Future experiments across contexts could disentangle these and other aspects of thalamic contextual modulation.

There are several limitations to our study which readily suggest future experiments in different contexts. One main limitation of our experimental design was the inability to record from the same neurons across each context. This concern is somewhat mitigated by the fact that, in the majority of our experiments, recordings in each context were performed within the same mice within days of each other, and within animal, the effects of context were consistent (data not shown; $p < 0.05$ for spontaneous and onset latency differences between contexts in N=5 experiments). Future experiments utilizing chronic extracellular recordings in dLGN or imaging of dLGN activity would enable the comparison of the same neurons in one context versus another. A second limitation is that the contextual effects described here could be explained by factors that were not observable in our experiments (e.g., subtle postural adjustments) that are themselves independent from facial movements, yet do not cause changes in the electrophysiological signatures of brain state in the visual system. These possibilities would require continuous monitoring whole-body movements and brain-wide signatures of arousal[64].

In summary, we revealed that the overall physical environment shapes basic features of visual processing in the thalamus. Contextual effects are typically thought to be strongest in cortex[32,33,65,66] so why might contextual modulation of LGN convey ecological advantages? In freely behaving mice, stationary epochs are naturally punctuated by running behaviors, such as during prey-capture and escape[12,13]. The visual system may thus be tuned to process information more quickly even when mice are totally still, so that ensuing visual processing during locomotion is already primed for integration of higher temporal frequencies, optic flow, etc. It would be most beneficial to accelerate the timing of visual signals at the earliest stage, rather than individually in multiple downstream structures. This quickened regime on the wheel is not readily observable in an experimental context (tube) that nonetheless surveys the system in comparable motor and arousal states. However, by limiting the potential for locomotion, the tube context minimizes widespread neural effects that may pose other interpretational complications for the experimental question at hand, such as psychometric studies of stimulus detection[3,7,20,21]. Overall, our findings highlight that the experimental choice of physical environmental context can have large impacts on the most basic aspects of visual processing, even as early as the primary visual thalamus. The information about environmental context sculpts baseline activity, response timing, and spatial information, allowing for more integrative processing of contextually relevant visual information to be broadcast to the rest of the visual system. More broadly, our findings imply that inherent properties of the environmental context could have marked effects on setting the neural information processing regime across other sensory systems.

Acknowledgements

We thank Tony Lien and Elaida Dimwamwa for feedback. This work was supported by National Eye Institute (F31EY033691 to K.P.), National Institute of Neurological Disorders and Stroke (T32NS096050 to K.P.; R01NS109978, RF1NS132288 to B.H.)

Author Contributions

K.P. performed all experiments, wrote code and analyzed data; K.P., B.H. wrote the manuscript.

Declaration of interests

The authors declare no competing interests.

Lead contact

Further information and requests for resources should be directed to the lead contact, Bilal Haider (bilal.haider@bme.gatech.edu).

Materials, Data, Code availability

This study did not generate new unique reagents. All data structures and code that generated each figure will be publicly available at DOI: 10.6084/m9.figshare.26364601 upon publication and linked from the corresponding author's institutional webpage.

Methods

Experimental subject details

Reagent or Resource	Source	Identifier	Number of Mice	Number of Recordings [wheel;tube]
Experimental Models: Organisms/Strains				
Mouse C57BL/6J	**Jackson Laboratory**	IMSR_JAX:000664	8	[7;17]
Mouse Ai32 x Scnn1a-Cre	**Jackson Laboratory**	IMSR_JAX:009613	1	[0;1]

All experimental procedures were approved by the Institutional Animal Care and Use Committee (IACUC) at the Georgia Institute of Technology

Implant surgery

Male C57BL/6J or Ai32 x Scnn1a-Cre mice (5-8 weeks old, individually housed in a reverse light cycle room, bred in-house) were implanted with a custom-built stainless steel head plate containing a recording chamber (3 mm in diameter) during isoflurane anesthesia (3% induction, 1-2% maintenance). The head plate was fixed to the skull using a layer of veterinary adhesive (VetBond) before being secured to the cranium with dental cement (Metabond). The recording chamber was sealed using an elastomer (KwikCast). Following implantation, mice were given a minimum of 3 days to fully recover.

Habituation to recording apparatus

Mice in the tube context were gently handled and habituated to the recording environment for a minimum of three days prior to experimentation. Mice in the wheel context were gently handled and habituated to the recording environment for a minimum of five days prior to experimentation, including habituation to the tube context. Mice were given a full three hours on the circular treadmill for at least three days (up to five) prior to recording.

Visual stimulus properties

Stimulus Display

Visual stimuli were displayed on gamma-corrected LCD displays (Dell Ultrasharp U2417H or U2419H, 60 Hz refresh rate) with a peak luminance of 250 cd * m^{-2}. Two displays were positioned at right angles to one another such that stimuli at 0° and 90° in azimuthal space have similar viewing angles relative to the mouse's eye. To confirm linearization, we displayed full contrast stimuli (full black to full white) and measured the resulting monitor luminance values with a photodiode (Thorlabs), then corrected this relationship with the (inverse) exponential function. We measured light levels using a photometer (AEMC CA811) with spectral sensitivity range (500 – 620 nm) overlapping the peak absorption wavelengths for both rods and M-cones, positioned at the same viewing angle as the mice. Measurements from the experimental apparatus was averaged (±SD); stimuli at [100% black, 50% gray background, 100% white] stimuli provided [0, 117.5 ± 14.4, 237.3 ± 28.7] cd * sr * m^{-2}.

Visual stimuli: Full Screen Flash

Stimuli were created using Matlab (2017b, 2019a) with the Psychophysics toolbox. Full screen flashes spanned from ~ − 60° to + 150° in azimuth. Stimuli consisted of a background of mean luminance (gray) for 0.25 s followed by either black (minimum luminance) or white (maximum luminance) screen for 0.25 s. Each full screen flash session consisted of 500-1000 trials (Fig. S1).

Visual stimuli: Receptive Field Mapping

Stimuli were created using Matlab (2017b, 2019a) with the Psychophysics toolbox. Receptive field (RF) mapping stimuli consisted of individually presented black (minimum luminance) or white (maximum luminance) against a gray background of mean luminance. Each square was 7°x7° and appeared in one of 160 spatial locations covering 90° (azimuth) x 50° (elevation), spanning the monocular and binocular visual field. Each stimulus was presented randomly across the 160 given stimulus locations, such that the same square would not appear in the same location on the subsequent trial. Stimuli were displayed for 0.1 s followed by a 0.3 s inter-stimulus interval. Stimuli were presented in blocks of trials, such that a block consisted of a single luminance of the square, and

each square was presented in each location 10 times within one block. Each experiment consisted of 10-30 repeats of square stimuli of either black or white in each spatial location.

Recordings

Recordings: dLGN and visual cortex

dLGN was targeted with stereotaxic coordinates (-2.5 mm posterior to bregma; -2.5 mm lateral from midline[67]. Each recording electrode contains a total of 960 channels, of which a subset of 383 were used for recording. Spikes were acquired at 30 kHz and local field potential (LFP) at 2.5 kHz via a PXIe Card, a National Instruments board, and Spike GLX software. In all experiments, a full field flash stimulus was shown while advancing to dLGN (2.8 - 3.2 mm below the dura) to confirm visual responses, and in most instances confirmed with histology.

Recordings: Eye camera

Face and eye movements were monitored by illuminating the animal's face and eye with infrared light (Mightex, SLS-02008-A). The right eye was monitored with a camera (Imaging source DMK 21Bu04.H) fitted with a zoom lens (Navitar 7000) and a long-pass filter (Mightex, 092/52x0.75). The camera was placed ~22 cm from the animal's right eye. Videos were obtained at 30 Hz.

Recordings: Locomotion

In wheel experiments, mice were free to run on a circular treadmill. The circular treadmill contained four equally spaced dowels around the perimeter. Running events were measured by an optical detector that triggers events following an IR beam break. As the wheel rotated, the dowels caused rapid beam breaks and triggered pulses. Running speed was quantified as the circumference of the wheel divided by the rate of trigger pulses per second. Trials were considered as locomoting if the calculated speed exceeded 1 cm/s for $\geq$ 1 s; trials were considered stationary when the speed was 0 cm/s for $\geq$ 1 s. Based on these metrics, each trial was categorized as: 1) stationary, 2) locomotion, 3) within 1 s of locomotion onset, 4) within 1 s of locomotion offset. Trials that did not meet these criteria (running onsets/offsets; trial types 3 and 4) were excluded from analysis (11% of trials; Fig S3E).

Recordings: Atropine

For recordings during atropine application (Fig. S3D,E), 1-3 drops of 1% Atropine Sulfate solution (Alcon) were applied topically on the eye. Recordings were performed after the pupil was fully and stably dilated, ~30 minutes after application. Full screen flash stimuli (both black and white) were presented to ensure the lack of light-induced pupillary responses.

Data Analysis

Data analysis: Spike sorting

Single units in dLGN were isolated and identified using Kilosort2[68]. Manual curation of clusters was performed using Phy2[69]. Clusters were chosen if the refractory period violations (occurring within 2 ms) occurred in fewer than 1% of all spikes assigned to a cluster[70].

Data analysis: Local Field Potential

A single-shank Neuropixels 1.0 electrode was used to simultaneously record the local field potential (LFP) in visual cortex and single unit activity in dLGN (Fig. 1C). Here, visual cortex was either the binocular portion of primary visual cortex (V1), rostrolateral (RL), or anterolateral (AL)[71] higher visual cortex. Visual responses to full screen flash stimuli were confirmed by inspecting the real-time neural data streaming during recordings, but the exact area boundaries and retinotopy of recorded regions within the visual cortical areas were not ascertained. We used LFP delta power in the visual cortex as a measure of changes in arousal. We used the spectrogram function in Matlab (Mathworks) and defined delta power as the power in the 1 to 4 Hz frequency band. We calculated the power over a sliding 1 s window with a 90% overlap to achieve 0.1 s precision. Next, we normalized the power spectrum by the sum across all frequencies at each time point, giving the relative power in the delta band[17]. We then smoothed the resulting delta power vector over a 1 s window. Pre-stimulus delta power was then calculated for each trial.

Data analysis: Arousal Level

Defining levels of arousal

In order to control for arousal level, the pre-stimulus delta power distribution was taken where the data had the greatest overlap between the tube and wheel context, which occurred at a moderate level of arousal (0.03 – 0.08 normalized delta power; full range: 0-0.15 normalized delta power) (Fig 1E).

Pre-stimulus delta power was calculated across all recordings for both contexts and plotted as a histogram (Fig. 3A). The histogram was then split into five equally sized bins, denoting the five increasing levels of arousal. When defining arousal levels within each context, the same bin widths and delta power values was used to define each level of arousal.

Data analysis: Pupil and periocular movements

To fit pupil size and calculate eye position, we used DeepLabCut[72]. Pupil size was tracked using eight points around the circumference of the pupil. Motion energy was calculated as the sum total of the absolute difference in pixel intensity between adjacent frames[48]. 8 points were fit around the eye from the bottom to top lid and the inner and outer corners. These pixels were excluded so that changes in pupil size do not contribute to the facial motion energy vector. At the end of every experimental session, mice were given liquid condensed milk while viewing a gray screen. Liquid consumption was chosen as a calibration event, because it evokes a large and standardized amount of motion energy and pupil dilation that is consistent between tube versus wheel experiments. In wheel experiments, we ensured mice were not actively running prior to consuming the milk, and during consumption animals were not actively running. We used the maximally evoked pupil area during consumption to normalize all pupil sizes as a fraction of the maximum evoked by reward consumption. We also normalized motion energy values to the same event, and normalized all motion energy values to the maximum motion energy value during consumption.

Data analysis: Permutation test

Surrogate datasets (Fig 2G) were created by first randomly sub-sampling all units across recordings (with replacement, 40% of units). This procedure was performed the same number of times as the number of recordings in each context (17 datasets for tube, 6 datasets for wheel). We averaged the surrogate datasets to create a population RF map over time. The activity from the center pixel of the population RF map was selected and turned into a peri-stimulus time histogram. Test statistics were calculated for onset latency, peak latency, and response duration between tube and wheel. 500 permutations were performed. A p value was calculated by counting the number of test statistics greater than the initial test statistic, divided by 500. A result was significant at $p < 0.05$.

Data analysis: ON/OFF classification in dLGN

Neurons in dLGN were classified as having ON or OFF preference from the response to black or white squares flashed in the neuron's receptive field. The number of spikes evoked by the change in luminance (40 – 140 ms after stimulus onset) were counted and used to calculate the ON/OFF index.

$$\text{ON/OFF index} = \frac{\text{Nspikes to ON}}{\text{Nspikes to ON} + \text{Nspikes to OFF}}$$

Neurons with an ON/OFF index of < 0.3 were identified as OFF cells and > 0.7 were ON dominant cells, as in previous studies[40,73]; wheel: 17 ON, 15 OFF, 40 mixed selectivity; tube: 72 ON, 48 OFF, 115 mixed).

Data analysis: dLGN Receptive Field Analysis

First, grand average receptive field (RF) maps were created for each neuron. RF maps were created by generating a 2D histogram of spike counts for every neuron at each of the 160 spatial locations of the mapping stimulus. Maps were binned at 0.01 s. Both black and white responses were combined to create grand average RF maps. The average response between 0.04 – 0.14 s after stimulus onset was taken for every unit to create a receptive field map[74]. A Chi-squared test for independence was used to determine whether a map had locations with significant ($p < 0.05$) responses above baseline that together defined the receptive field[66]. Except for Fig. S1 (all visually responsive dLGN neurons), only those neurons with a significant spatial RF map were analyzed in this report (43% of all recorded neurons with visual responses to full screen flashes also passed significance criteria for 2-D RF maps, consistent with prior work[66]).

Data analysis: Arousal-based Receptive Field Maps

To create arousal-based RF maps, the grand average RF maps were separated by trial type. Each trial was assigned a pre-stimulus delta power value over the 1s prior to stimulus onset within the RF. The distribution of delta power over all experiments was taken and separated into three equally sized bins to determine 'low', 'mid', and 'high' levels of delta power. Trials that fell into each category were then taken to create the arousal-based maps for each neuron (Fig. 4 F, G; example maps from matched arousal trials as in Figs 1,2).

Data analysis: Receptive Field Center Size

To calculate receptive field center size, individual receptive field maps were first baseline subtracted (0.1 s pre-stimulus activity) and the center of the receptive field was identified as the spatial location where the most spikes were evoked to the presentation of the sparse noise visual stimulus. Any pixels contiguous with the center pixel that evoked spikes at greater than or equal to 50% of the maximally evoked center pixel were included as part of the receptive field. Area was calculated assuming circularity ($A = \pi r^2$). Eye movements still occur in stationary animals, although to a lesser degree[11,75]. Therefore, we also restricted our receptive field analysis to trials where the eye position deviated less than the size of the visual stimulus (within 7° of the average central position across the recording, as in[11]). This excluded just 4.3% of trials on the tube, and 2% of all stationary trials on the wheel.

Data analysis: Spatial Selectivity

To calculate receptive field spatial selectivity, we used a modulation index (MI) to assess firing at the center of the receptive field relative to the background for each individual neuron. Using the same 'center' pixels as identified for the receptive field, the average firing rate in the receptive field was calculated for all of these, while all other pixels (typically 155-159 outside of the center; from 160 total pixels in a single RF map) were taken as background. Here, we did not baseline-subtract the receptive field maps in order to capture the differences in the actual firing rates within neuron.

$$MI = \frac{[center] - [background]}{[center] + [background]}$$

Data analysis: Quantifying visual response amplitude and timing

All peri-stimulus time histograms (PSTH) had a bin size of 0.01 s. Due to inherent variability and sampling constraints, neurons with significant RF maps could nonetheless fail to have a stimulus appear in the receptive field during a particular condition (e.g., stationary trials within one of the five binned levels of arousal). To calculate baseline firing (Fig 2B, Fig 3 D-F), we took all neurons that had a significant receptive field map (n=276 tube, n=107 wheel). For all other stimulus-evoked analysis, the response to the best stimulus location and preferred color (black or white) was taken for each neuron. When analyzing baseline activity for those subsets of neurons that also had a response to the best stimulus location within a particular condition, we still observed a significant effect of context on baseline activity (data not shown). If a neuron was not statistically categorized as ON or OFF (i.e., mixed selectivity), average responses to both black and white stimuli were analyzed. Baseline activity (Fig. 2B; Fig 3D E, F) was calculated in the 0.1 s prior to stimulus onset. Baseline-subtracted peak visual response (Fig. 2C; Fig. 3G-I) was calculated by subtracting the baseline activity (0.1 s prior to stimulus onset) from the average firing rate in a 0.05 s window 0.04 s after stimulus onset. The onset latency (Fig. 2D; Fig. 3J) was calculated as the earliest time after stimulus onset during which baseline-subtracted cumulative PSTH was above a 95% bootstrapped confidence interval on the cumulative baseline values[76]. The peak response latency (Fig. 2E, Fig. 3K) was the time at the maximum evoked response for each individual neuron. The response duration (Fig. 2F, Fig. 3L) was quantified by assessing the duration of the interval in which the response was at or above 25% of the maximum firing rate. A few neurons with response durations >0.2 s were excluded from analysis (1/72 units on wheel, 3/235 units on tube).

Histology

At the end of experiments, lipophilic dye (DiI, Invitrogen) was painted on the back of the electrode and inserted in dLGN for a minimum of 2.5 hours. Animals were transcardially perfused with 4% paraformaldehyde (PFA, VWR) in 1x PBS. Brains were kept in 4% PFA in 1x PBS for 24 hours and transferred to PBS. Brains were sectioned (100 um) on a Vibratome (Leica). Brains were then stained with DAPI (2 mM in PBS, AppliChem). We then mounted each slide with a fluorescent mounting medium (Vectashield, Vector Labs). Sections were imaged using a Confocal microscope (Zeiss). Targeting of dLGN was confirmed post-mortem, and any data obtained from mice where we observed a recording track outside of dLGN was discarded.

References

1. Livingstone, M.S., and Hubel, D.H. (1981). Effects of sleep and arousal on the processing of visual information in the cat. Nature *291*, 554-561. 10.1038/291554a0.
2. Vinck, M., Batista-Brito, R., Knoblich, U., and Cardin, J.A. (2015). Arousal and locomotion make distinct contributions to cortical activity patterns and visual encoding. Neuron *86*, 740-754. 10.1016/j.neuron.2015.03.028.
3. Neske, G.T., Nestvogel, D., Steffan, P.J., and McCormick, D.A. (2019). Distinct Waking States for Strong Evoked Responses in Primary Visual Cortex and Optimal Visual Detection Performance. J Neurosci *39*, 10044-10059. 10.1523/JNEUROSCI.1226-18.2019.
4. Lee, J.J., Krumin, M., Harris, K.D., and Carandini, M. (2022). Task specificity in mouse parietal cortex. Neuron *110*, 2961-2969 e2965. 10.1016/j.neuron.2022.07.017.
5. Niell, C.M., and Stryker, M.P. (2010). Modulation of visual responses by behavioral state in mouse visual cortex. Neuron *65*, 472-479. 10.1016/j.neuron.2010.01.033.
6. Keller, G.B., Bonhoeffer, T., and Hubener, M. (2012). Sensorimotor mismatch signals in primary visual cortex of the behaving mouse. Neuron *74*, 809-815. 10.1016/j.neuron.2012.03.040.
7. Bennett, C., Arroyo, S., and Hestrin, S. (2013). Subthreshold mechanisms underlying state-dependent modulation of visual responses. Neuron *80*, 350-357. 10.1016/j.neuron.2013.08.007.
8. Erisken, S., Vaiceliunaite, A., Jurjut, O., Fiorini, M., Katzner, S., and Busse, L. (2014). Effects of locomotion extend throughout the mouse early visual system. Curr Biol *24*, 2899-2907. 10.1016/j.cub.2014.10.045.
9. Gibson, J.J. (1979). The ecological approach to visual perception (Houghton Mifflin).
10. Pakan, J.M., Lowe, S.C., Dylda, E., Keemink, S.W., Currie, S.P., Coutts, C.A., and Rochefort, N.L. (2016). Behavioral-state modulation of inhibition is context-dependent and cell type specific in mouse visual cortex. Elife *5*. 10.7554/eLife.14985.
11. Saleem, A.B., Ayaz, A., Jeffery, K.J., Harris, K.D., and Carandini, M. (2013). Integration of visual motion and locomotion in mouse visual cortex. Nat Neurosci *16*, 1864-1869. 10.1038/nn.3567.
12. Hoy, J.L., Yavorska, I., Wehr, M., and Niell, C.M. (2016). Vision Drives Accurate Approach Behavior during Prey Capture in Laboratory Mice. Curr Biol *26*, 3046-3052. 10.1016/j.cub.2016.09.009.
13. Yilmaz, M., and Meister, M. (2013). Rapid innate defensive responses of mice to looming visual stimuli. Curr Biol *23*, 2011-2015. 10.1016/j.cub.2013.08.015.
14. Liang, F., Xiong, X.R., Zingg, B., Ji, X.Y., Zhang, L.I., and Tao, H.W. (2015). Sensory Cortical Control of a Visually Induced Arrest Behavior via Corticotectal Projections. Neuron *86*, 755-767. 10.1016/j.neuron.2015.03.048.
15. Zhao, X., Liu, M., and Cang, J. (2014). Visual cortex modulates the magnitude but not the selectivity of looming-evoked responses in the superior colliculus of awake mice. Neuron *84*, 202-213. 10.1016/j.neuron.2014.08.037.
16. Veit, J., Handy, G., Mossing, D.P., Doiron, B., and Adesnik, H. (2023). Cortical VIP neurons locally control the gain but globally control the coherence of gamma band rhythms. Neuron *111*, 405-417 e405. 10.1016/j.neuron.2022.10.036.
17. Reinhold, K., Resulaj, A., and Scanziani, M. (2023). Brain State-Dependent Modulation of Thalamic Visual Processing by Cortico-Thalamic Feedback. J Neurosci *43*, 1540-1554. 10.1523/JNEUROSCI.2124-21.2022.
18. Lee, A.M., Hoy, J.L., Bonci, A., Wilbrecht, L., Stryker, M.P., and Niell, C.M. (2014). Identification of a brainstem circuit regulating visual cortical state in parallel with locomotion. Neuron *83*, 455-466. 10.1016/j.neuron.2014.06.031.
19. Sachidhanandam, S., Sreenivasan, V., Kyriakatos, A., Kremer, Y., and Petersen, C.C. (2013). Membrane potential correlates of sensory perception in mouse barrel cortex. Nat Neurosci *16*, 1671-1677. 10.1038/nn.3532.
20. Speed, A., Del Rosario, J., Mikail, N., and Haider, B. (2020). Spatial attention enhances network, cellular and subthreshold responses in mouse visual cortex. Nat Commun *11*, 505. 10.1038/s41467-020-14355-4.
21. Oryshchuk, A., Sourmpis, C., Weverbergh, J., Asri, R., Esmaeili, V., Modirshanechi, A., Gerstner, W., Petersen, C.C.H., and Crochet, S. (2024). Distributed and specific encoding of sensory, motor, and decision information in the mouse neocortex during goal-directed behavior. Cell Rep *43*, 113618. 10.1016/j.celrep.2023.113618.
22. Dimwamwa, E.D., Pala, A., Chundru, V., Wright, N.C., and Stanley, G.B. (2024). Dynamic corticothalamic modulation of the somatosensory thalamocortical circuit during wakefulness. Nat Commun *15*, 3529. 10.1038/s41467-024-47863-8.

23. Burgess, C.P., Lak, A., Steinmetz, N.A., Zatka-Haas, P., Bai Reddy, C., Jacobs, E.A.K., Linden, J.F., Paton, J.J., Ranson, A., Schroder, S., et al. (2017). High-Yield Methods for Accurate Two-Alternative Visual Psychophysics in Head-Fixed Mice. Cell Rep *20*, 2513-2524. 10.1016/j.celrep.2017.08.047.

24. Musall, S., Sun, X.R., Mohan, H., An, X., Gluf, S., Li, S.J., Drewes, R., Cravo, E., Lenzi, I., Yin, C., et al. (2023). Pyramidal cell types drive functionally distinct cortical activity patterns during decision-making. Nat Neurosci *26*, 495-505. 10.1038/s41593-022-01245-9.

25. Musall, S., Kaufman, M.T., Juavinett, A.L., Gluf, S., and Churchland, A.K. (2019). Single-trial neural dynamics are dominated by richly varied movements. Nat Neurosci *22*, 1677-1686. 10.1038/s41593-019-0502-4.

26. International Brain, L., Aguillon-Rodriguez, V., Angelaki, D., Bayer, H., Bonacchi, N., Carandini, M., Cazettes, F., Chapuis, G., Churchland, A.K., Dan, Y., et al. (2021). Standardized and reproducible measurement of decision-making in mice. Elife *10*. 10.7554/eLife.63711.

27. Bereshpolova, Y., Stoelzel, C.R., Zhuang, J., Amitai, Y., Alonso, J.M., and Swadlow, H.A. (2011). Getting drowsy? Alert/nonalert transitions and visual thalamocortical network dynamics. J Neurosci *31*, 17480-17487. 10.1523/JNEUROSCI.2262-11.2011.

28. Lee, S.H., and Dan, Y. (2012). Neuromodulation of brain states. Neuron *76*, 209-222. 10.1016/j.neuron.2012.09.012.

29. Pinto, L., Goard, M.J., Estandian, D., Xu, M., Kwan, A.C., Lee, S.H., Harrison, T.C., Feng, G., and Dan, Y. (2013). Fast modulation of visual perception by basal forebrain cholinergic neurons. Nat Neurosci *16*, 1857-1863. 10.1038/nn.3552.

30. Polack, P.O., Friedman, J., and Golshani, P. (2013). Cellular mechanisms of brain state-dependent gain modulation in visual cortex. Nat Neurosci *16*, 1331-1339. 10.1038/nn.3464.

31. Fu, Y., Tucciarone, J.M., Espinosa, J.S., Sheng, N., Darcy, D.P., Nicoll, R.A., Huang, Z.J., and Stryker, M.P. (2014). A cortical circuit for gain control by behavioral state. Cell *156*, 1139-1152. 10.1016/j.cell.2014.01.050.

32. Gilbert, C.D., and Li, W. (2013). Top-down influences on visual processing. Nat Rev Neurosci *14*, 350-363. 10.1038/nrn3476.

33. Zhang, S., Xu, M., Kamigaki, T., Hoang Do, J.P., Chang, W.C., Jenvay, S., Miyamichi, K., Luo, L., and Dan, Y. (2014). Selective attention. Long-range and local circuits for top-down modulation of visual cortex processing. Science *345*, 660-665. 10.1126/science.1254126.

34. Liang, L., Fratzl, A., Reggiani, J.D.S., El Mansour, O., Chen, C., and Andermann, M.L. (2020). Retinal Inputs to the Thalamus Are Selectively Gated by Arousal. Curr Biol *30*, 3923-3934 e3929. 10.1016/j.cub.2020.07.065.

35. Spacek, M.A., Crombie, D., Bauer, Y., Born, G., Liu, X., Katzner, S., and Busse, L. (2022). Robust effects of corticothalamic feedback and behavioral state on movie responses in mouse dLGN. Elife *11*. 10.7554/eLife.70469.

36. Aydin, C., Couto, J., Giugliano, M., Farrow, K., and Bonin, V. (2018). Locomotion modulates specific functional cell types in the mouse visual thalamus. Nat Commun *9*, 4882. 10.1038/s41467-018-06780-3.

37. Nestvogel, D.B., and McCormick, D.A. (2022). Visual thalamocortical mechanisms of waking state-dependent activity and alpha oscillations. Neuron *110*, 120-138 e124. 10.1016/j.neuron.2021.10.005.

38. Saleem, A.B., Lien, A.D., Krumin, M., Haider, B., Roson, M.R., Ayaz, A., Reinhold, K., Busse, L., Carandini, M., and Harris, K.D. (2017). Subcortical Source and Modulation of the Narrowband Gamma Oscillation in Mouse Visual Cortex. Neuron *93*, 315-322. 10.1016/j.neuron.2016.12.028.

39. Storchi, R., Bedford, R.A., Martial, F.P., Allen, A.E., Wynne, J., Montemurro, M.A., Petersen, R.S., and Lucas, R.J. (2017). Modulation of Fast Narrowband Oscillations in the Mouse Retina and dLGN According to Background Light Intensity. Neuron *93*, 299-307. 10.1016/j.neuron.2016.12.027.

40. Shin, D., Peelman, K., Lien, A.D., Del Rosario, J., and Haider, B. (2023). Narrowband gamma oscillations propagate and synchronize throughout the mouse thalamocortical visual system. Neuron *111*, 1076-1085 e1078. 10.1016/j.neuron.2023.03.006.

41. Steriade, M., McCormick, D.A., and Sejnowski, T.J. (1993). Thalamocortical oscillations in the sleeping and aroused brain. Science *262*, 679-685. 10.1126/science.8235588.

42. Timofeev, I., and Steriade, M. (1996). Low-frequency rhythms in the thalamus of intact-cortex and decorticated cats. J Neurophysiol *76*, 4152-4168. 10.1152/jn.1996.76.6.4152.

43. McGinley, M.J., Vinck, M., Reimer, J., Batista-Brito, R., Zagha, E., Cadwell, C.R., Tolias, A.S., Cardin, J.A., and McCormick, D.A. (2015). Waking State: Rapid Variations Modulate Neural and Behavioral Responses. Neuron *87*, 1143-1161. 10.1016/j.neuron.2015.09.012.

44. Adesnik, H., Bruns, W., Taniguchi, H., Huang, Z.J., and Scanziani, M. (2012). A neural circuit for spatial summation in visual cortex. Nature *490*, 226-231. 10.1038/nature11526.

45. Pluta, S., Naka, A., Veit, J., Telian, G., Yao, L., Hakim, R., Taylor, D., and Adesnik, H. (2015). A direct translaminar inhibitory circuit tunes cortical output. Nat Neurosci *18*, 1631-1640. 10.1038/nn.4123.

46. Veit, J., Hakim, R., Jadi, M.P., Sejnowski, T.J., and Adesnik, H. (2017). Cortical gamma band synchronization through somatostatin interneurons. Nat Neurosci *20*, 951-959. 10.1038/nn.4562.

47. Haider, B., Schulz, D.P., Hausser, M., and Carandini, M. (2016). Millisecond Coupling of Local Field Potentials to Synaptic Currents in the Awake Visual Cortex. Neuron *90*, 35-42. 10.1016/j.neuron.2016.02.034.

48. Stringer, C., Pachitariu, M., Steinmetz, N., Reddy, C.B., Carandini, M., and Harris, K.D. (2019). Spontaneous behaviors drive multidimensional, brainwide activity. Science *364*, 255. 10.1126/science.aav7893.

49. Crombie, D., Spacek, M.A., Leibold, C., and Busse, L. (2024). Spiking activity in the visual thalamus is coupled to pupil dynamics across temporal scales. PLoS Biol *22*, e3002614. 10.1371/journal.pbio.3002614.

50. Durand, S., Iyer, R., Mizuseki, K., de Vries, S., Mihalas, S., and Reid, R.C. (2016). A Comparison of Visual Response Properties in the Lateral Geniculate Nucleus and Primary Visual Cortex of Awake and Anesthetized Mice. J Neurosci *36*, 12144-12156. 10.1523/JNEUROSCI.1741-16.2016.

51. Mazer, J.A., Vinje, W.E., McDermott, J., Schiller, P.H., and Gallant, J.L. (2002). Spatial frequency and orientation tuning dynamics in area V1. Proc Natl Acad Sci U S A *99*, 1645-1650. 10.1073/pnas.022638499.

52. McCormick, D.A., and Prince, D.A. (1987). Acetylcholine causes rapid nicotinic excitation in the medial habenular nucleus of guinea pig, in vitro. J Neurosci *7*, 742-752. 10.1523/JNEUROSCI.07-03-00742.1987.

53. Goard, M., and Dan, Y. (2009). Basal forebrain activation enhances cortical coding of natural scenes. Nat Neurosci *12*, 1444-1449. 10.1038/nn.2402.

54. Roberts, M.J., Zinke, W., Guo, K., Robertson, R., McDonald, J.S., and Thiele, A. (2005). Acetylcholine dynamically controls spatial integration in marmoset primary visual cortex. J Neurophysiol *93*, 2062-2072. 10.1152/jn.00911.2004.

55. Ayaz, A., Saleem, A.B., Scholvinck, M.L., and Carandini, M. (2013). Locomotion controls spatial integration in mouse visual cortex. Curr Biol *23*, 890-894. 10.1016/j.cub.2013.04.012.

56. Lu, S.M., Guido, W., and Sherman, S.M. (1993). The brain-stem parabrachial region controls mode of response to visual stimulation of neurons in the cat's lateral geniculate nucleus. Vis Neurosci *10*, 631-642. 10.1017/s0952523800005332.

57. Sillito, A.M., and Kemp, J.A. (1983). Cholinergic modulation of the functional organization of the cat visual cortex. Brain Res *289*, 143-155. 10.1016/0006-8993(83)90015-x.

58. McCormick, D.A. (1992). Cellular mechanisms underlying cholinergic and noradrenergic modulation of neuronal firing mode in the cat and guinea pig dorsal lateral geniculate nucleus. J Neurosci *12*, 278-289. 10.1523/JNEUROSCI.12-01-00278.1992.

59. Funke, K., Pape, H.C., and Eysel, U.T. (1993). Noradrenergic modulation of retinogeniculate transmission in the cat. J Physiol *463*, 169-191. 10.1113/jphysiol.1993.sp019590.

60. Augustinaite, S., and Kuhn, B. (2020). Complementary Ca(2+) Activity of Sensory Activated and Suppressed Layer 6 Corticothalamic Neurons Reflects Behavioral State. Curr Biol *30*, 3945-3960 e3945. 10.1016/j.cub.2020.07.069.

61. Born, G., Schneider-Soupiadis, F.A., Erisken, S., Vaiceliunaite, A., Lao, C.L., Mobarhan, M.H., Spacek, M.A., Einevoll, G.T., and Busse, L. (2021). Corticothalamic feedback sculpts visual spatial integration in mouse thalamus. Nat Neurosci *24*, 1711-1720. 10.1038/s41593-021-00943-0.

62. Xing, D., Yeh, C.I., Gordon, J., and Shapley, R.M. (2014). Cortical brightness adaptation when darkness and brightness produce different dynamical states in the visual cortex. Proc Natl Acad Sci U S A *111*, 1210-1215. 10.1073/pnas.1314690111.

63. Tucker, T.R., and Fitzpatrick, D. (2006). Luminance-evoked inhibition in primary visual cortex: a transient veto of simultaneous and ongoing response. J Neurosci *26*, 13537-13547. 10.1523/JNEUROSCI.3723-06.2006.

64. Marshall, J.D., Aldarondo, D.E., Dunn, T.W., Wang, W.L., Berman, G.J., and Olveczky, B.P. (2021). Continuous Whole-Body 3D Kinematic Recordings across the Rodent Behavioral Repertoire. Neuron *109*, 420-437 e428. 10.1016/j.neuron.2020.11.016.

65. Gilbert, C.D., and Wiesel, T.N. (1990). The influence of contextual stimuli on the orientation selectivity of cells in primary visual cortex of the cat. Vision Res *30*, 1689-1701. 10.1016/0042-6989(90)90153-c.

66. Siegle, J.H., Jia, X., Durand, S., Gale, S., Bennett, C., Graddis, N., Heller, G., Ramirez, T.K., Choi, H., Luviano, J.A., et al. (2021). Survey of spiking in the mouse visual system reveals

functional hierarchy. Nature *592*, 86-92. 10.1038/s41586-020-03171-x.

67. Franklin, K.B.J., and Paxinos, G. (2013). Paxinos and Franklin's The mouse brain in stereotaxic coordinates, Fourth edition. Edition (Academic Press, an imprint of Elsevier).

68. Pachitariu, M., Steinmetz, N., Kadir, S., Carandini, M., and Kenneth D., H. (2016). Kilosort: realtime spike-sorting for extracellular electrophysiology with hundreds of channels. bioRxiv, 061481. 10.1101/061481.

69. Rossant, C., Kadir, S.N., Goodman, D.F.M., Schulman, J., Hunter, M.L.D., Saleem, A.B., Grosmark, A., Belluscio, M., Denfield, G.H., Ecker, A.S., et al. (2016). Spike sorting for large, dense electrode arrays. Nat Neurosci *19*, 634-641. 10.1038/nn.4268.

70. Hill, D.N., Mehta, S.B., and Kleinfeld, D. (2011). Quality metrics to accompany spike sorting of extracellular signals. J Neurosci *31*, 8699-8705. 10.1523/JNEUROSCI.0971-11.2011.

71. Nsiangani, A., Del Rosario, J., Yeh, A.C., Shin, D., Wells, S., Lev-Ari, T., Williams, B., and Haider, B. (2022). Optimizing intact skull intrinsic signal imaging for subsequent targeted electrophysiology across mouse visual cortex. Sci Rep *12*, 2063. 10.1038/s41598-022-05932-2.

72. Mathis, A., Mamidanna, P., Cury, K.M., Abe, T., Murthy, V.N., Mathis, M.W., and Bethge, M. (2018). DeepLabCut: markerless pose estimation of user-defined body parts with deep learning. Nat Neurosci *21*, 1281-1289. 10.1038/s41593-018-0209-y.

73. Schroder, S., Steinmetz, N.A., Krumin, M., Pachitariu, M., Rizzi, M., Lagnado, L., Harris, K.D., and Carandini, M. (2020). Arousal Modulates Retinal Output. Neuron *107*, 487-495 e489. 10.1016/j.neuron.2020.04.026.

74. Lien, A.D., and Scanziani, M. (2013). Tuned thalamic excitation is amplified by visual cortical circuits. Nat Neurosci *16*, 1315-1323. 10.1038/nn.3488.

75. Sakatani, T., and Isa, T. (2007). Quantitative analysis of spontaneous saccade-like rapid eye movements in C57BL/6 mice. Neurosci Res *58*, 324-331. 10.1016/j.neures.2007.04.003.

76. Wiest, M.C., Bentley, N., and Nicolelis, M.A. (2005). Heterogeneous integration of bilateral whisker signals by neurons in primary somatosensory cortex of awake rats. J Neurophysiol *93*, 2966-2973. 10.1152/jn.00556.2004.

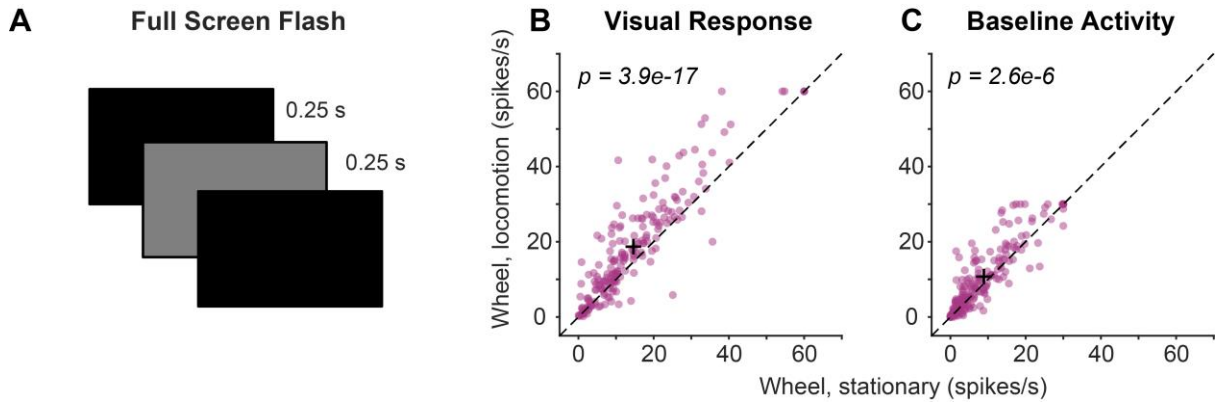

Supplementary Figure 1: Response to full screen flash during locomotion versus stationary trials

A. Full screen flash stimulus (grey to black illustrated here; grey to white also shown in experiments).
B. Visual response of dLGN neurons to a full screen flash stimulus is elevated during locomotion versus stationary epochs (N = 5 mice, n = 196 neurons, p = 3.9e-17; sign rank test).
C. Baseline activity of neurons during gray screen periods is elevated during locomotion versus stationary epochs (p = 2.6e-6; sign rank test).

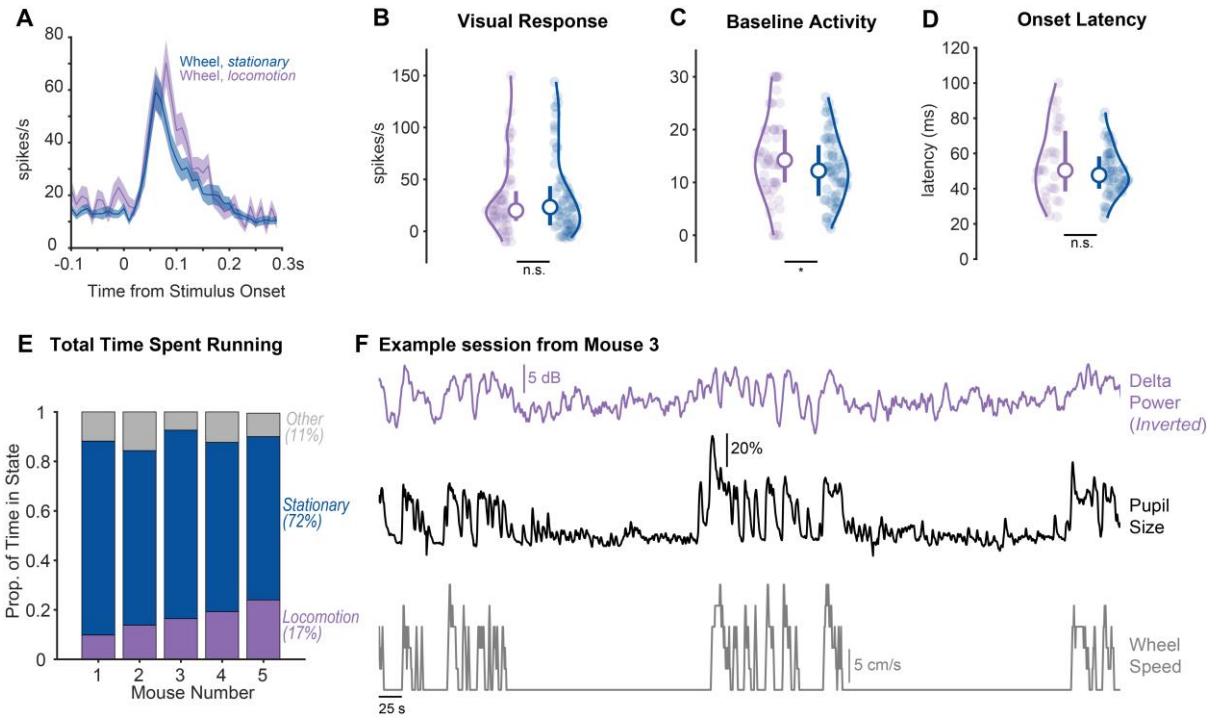

Supplementary Figure 2: Visual responses on wheel during locomotion versus stationary trials

A. Average dLGN spiking response on wheel during running (purple) vs. stationary (dark blue) trials when the best stimulus was presented in a given neuron's receptive field.
B. Visual response amplitude is similar between locomotion and stationary trials (locomotion: 20 ± 14 spikes/s, n = 64; stationary, 23 ± 18.5 spikes/s, n = 72; Median ± IQR/2; p = 0.494; Wilcoxon one-sided rank sum test throughout figure).
C. Baseline activity greater during locomotion versus stationary trials (run 14.2 ± 5.0 spikes/s, stationary 12.22 ± 5.2 spikes/s; p = 0.033).
D. Onset latency was comparable between locomotion and stationary trials (p = 0.204).
E. Example session over a single recording block (~12 minutes for a full block of squares tiling the visual hemifield). Traces show aligned visual cortical LFP delta power (inverted, purple), pupil size (black), and running wheel speed (gray).
F. Proportion of time spent running on average across all recording sessions for each given mouse recorded in the wheel. Across all recording days and mice, mice on average ran 17% of the time, and were stationary 72% of the time. On average, 11% of trials were excluded as uncategorized for either running or stationary criteria due to being within 1 s of a running onset/offset (see Methods).

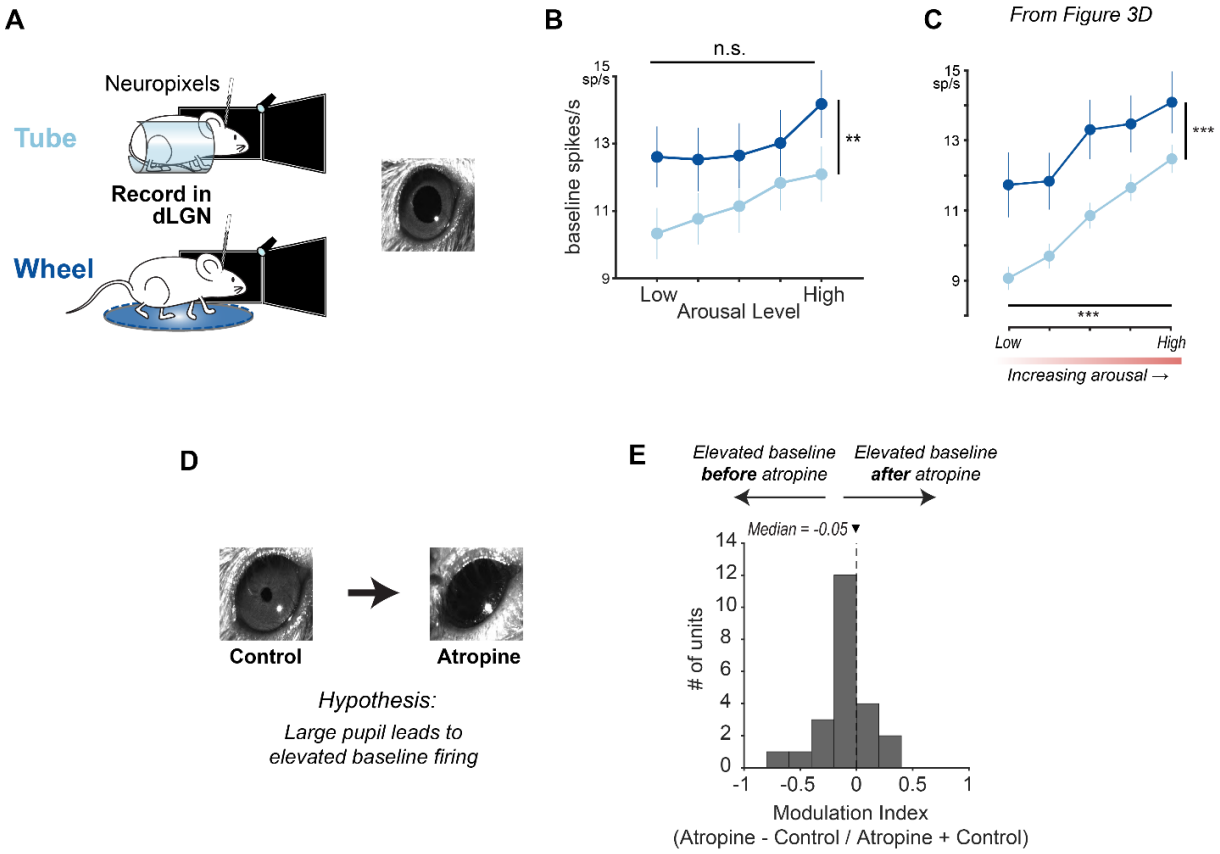

Supplementary Figure 3: Artificial dilation of pupil does not increase spontaneous firing rates

A. Experiments were performed on the tube and the wheel in full darkness to elicit maximal pupil dilation on all trials (N = 2 mice, tube; N = 2 mice, wheel).
B. Baseline activity on all stationary trials remained significantly elevated on the wheel relative to the tube (wheel n = 102 neurons, tube n = 90 neurons, $p = 0.0002$). There was no significant effect of increasing arousal on baseline activity in full darkness ($p = 0.3096$).
C. Data from Figure 3D when animals were in front of a gray screen.
D. Atropine was applied externally to mouse's eye to artificially dilate the pupil (n = 1 mouse, 23 neurons). If increased baseline firing is solely due to more light entering the eye with a large pupil, atropine should increase baseline firing relative to control. Note extreme dilation of pupil after atropine relative to baseline, and compared to full darkness (in A).
E. Baseline firing rates were not elevated when pupil was artificially dilated with atropine, relative to control firing rates in the same neurons before atropine application. Modulation expected to be positive if atropine increased baseline firing rates.

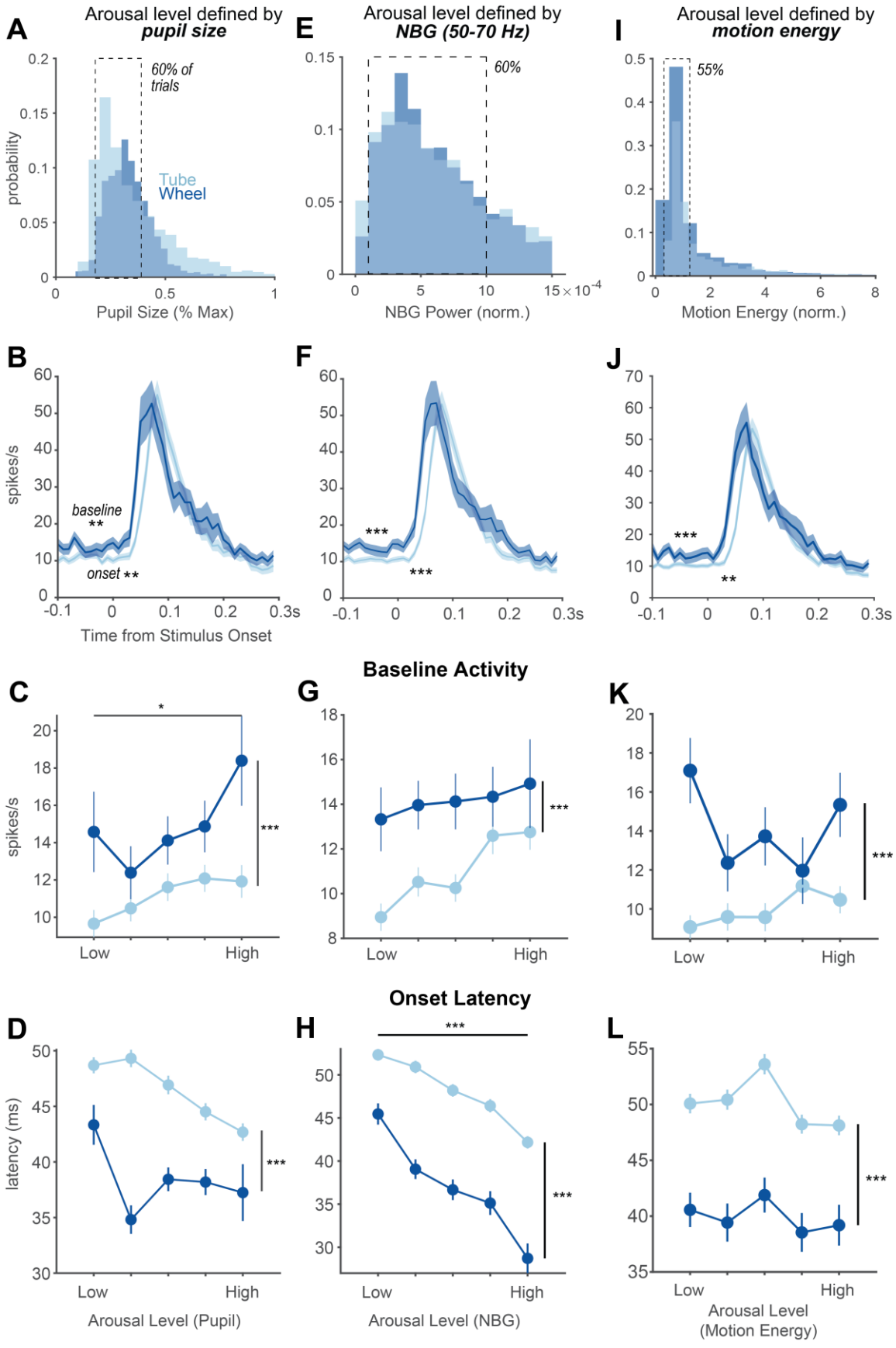

Supplementary Figure 4: Alternative methods to define arousal level using pupil size, narrowband gamma power (NBG), and motion energy.

A. Distribution of pre-stimulus pupil size across the tube (light) and wheel (dark) physical contexts. The central 60% of trials were analyzed.
B. Population peri-stimulus time histogram (PSTH) of neurons in dLGN when a given neuron's preferred stimulus is presented in the best location. Baseline activity was significantly elevated on the wheel relative to the tube (wheel n = 73, 12.9 ± 4.2 spikes/s; tube n = 219, 9.2 ± 5 spikes/s; p = 0.0016; Median ± IQR; Wilcoxon rank sum test; same neuron numbers and statistics throughout unless otherwise noted). Onset latency was faster in the wheel context (wheel 48 ± 7.5 ms; tube 56 ± 14 ms; p = 0.0021).
C. Baseline activity was overall elevated on the wheel relative to the tube (p = 8.8e-6) and increased with increasing arousal (p = 0.0303; two-way ANOVA).
D. Onset latency was overall faster in the wheel relative to the tube (p = 8e-10, two-way ANOVA). There was no significant effect of increasing arousal level on onset latency (p = 0.0725).
E. Same as in A, but for pre-stimulus narrowband gamma (50-70 Hz) power. The central 60% of trials were analyzed.
F. Same as in B. Baseline activity was significantly elevated on the wheel relative to the tube (wheel 12.0 ± 4.4 spikes/s, tube 8.8 ± 3.9 spikes/s; p = 7.2e-4)
G. Same as in C. Baseline activity was significantly elevated on the wheel relative to the tube (p = 8.7e-5). There was no significant effect of increasing arousal level on baseline activity (p = 0.1339; two-way ANOVA).
H. Onset latency was overall faster in the wheel relative to the tube (p = 5.5e-21, two-way ANOVA). Increasing arousal level resulted in faster onset latencies in both contexts (p = 6.2e-10).
I. Same as in A, E, but for pre-stimulus motion energy (Methods). The central 55% of trials were analyzed.
J. Same as in B, F. Baseline activity was significantly elevated on the wheel relative to the tube (wheel 14.0 ± 9.0 spikes/s, 10.1 ± 7.1 spikes/s*; p = 5.2e-4*). Onset latency was faster in the wheel (wheel 48 ± 7.5 ms; tube 56 ± 14 ms; p = 0.0078)
K. Baseline activity was elevated in the wheel relative to the tube (p = 2.0e-8) but was not impacted by increasing arousal level (p = 0.2164; two-way ANOVA).
L. Onset latency was overall faster in the wheel relative to the tube (p = 1.56e-14, two-way ANOVA). There was no significant effect of increasing arousal level on onset latency (p = 0.1799).